DOI: 10.1002/chem.200501249

A Range of Spin-Crossover Temperature $T_{1/2} > 300$ K Results from Out-of-Sphere Anion Exchange in a Series of Ferrous Materials Based on the 4-(4-Imidazolylmethyl)-2-(2-imidazolylmethyl)imidazole (trim) Ligand, $[Fe(trim)_2]X_2$ (X = F, Cl, Br, I): Comparison of Experimental Results with Those Derived from Density Functional Theory Calculations

Gilles Lemercier,[a, c] Nicolas Bréfuel,[a] Sergiu Shova,[a, e] Juliusz A. Wolny,[b, f] Françoise Dahan,[a] Marc Verelst,[a, d] Hauke Paulsen,*[b] Alfred X. Trautwein,*[b] and Jean-Pierre Tuchagues*[a]

Abstract: The synthesis and characterization of $[Fe^{II}(trim)_2]Cl_2$ (**2**), $[Fe^{II}(trim)_2]Br_2 \cdot MeOH$ (**3**), and $[Fe^{II}(trim)_2]I_2 \cdot MeOH$ (**4**), including the X-ray crystal structure determinations of **2** (50 and 293 K) and **4** (293 K), have been performed and their properties have been examined. In agreement with the magnetic susceptibility results, the Mössbauer data show the presence of high-spin (HS) to low-spin (LS) crossover with a range of $T_{1/2}$ larger than 300 K (from $\approx$20 K for $[Fe^{II}(trim)_2]F_2$ (**1**) to $\approx$380 K for **4**). All complexes in this series include the same $[Fe(trim)_2]^{2+}$ complex cation: the ligand field comprises a constant contribution from the trim ligands and a variable one originating from the out-of-sphere anions, which is transmitted to the metal center by the connecting imidazole rings and hydrogen bonds. The impressive variation in the intrinsic characteristics of the spin-crossover (SCO) phenomenon in this series is then interpreted as an inductive effect of the anions transmitted to the nitrogen donors through the hydrogen bonds. Based on this qualitative analysis, an increased inductive effect of the out-of-sphere anion corresponds to a decreased SCO temperature $T_{1/2}$, in agreement with the experimental results. Electronic structure calculations with periodic boundary conditions have been performed that show the importance of intermolecular effects in tuning the ligand field, and thus in determining the transition temperature. Starting with the geometries obtained from the X-ray studies, the $[Fe^{II}(trim)_2]X_2$ complex molecules **1**–**4** have been investigated both for the single molecules and the crystal lattices with the local density approximation of density functional theory. The bulk geometries of the complex cations deduced from the X-ray studies and those calculated are in fair agreement for both approaches. However, the trend observed for the transition temperatures of **1**–**4** disagrees with the trend for the spin-state splittings E_S (difference $E_{HS}-E_{LS}$ between the energy of the HS and LS isomers) calculated for the isolated molecules, whereas it agrees with the trend for E_S calculated with periodic boundary conditions. The latter calculations predict the strongest stabilization of the HS state for the fluoride complex, which actually is essentially HS above $T = 50$ K, while the most pronounced stabilization of the LS state is predicted for **4**, in line with the experimental results.

Keywords: density functional calculations · ion exchange · iron · Moessbauer spectroscopy · spin crossover

[a] G. Lemercier, Dr. N. Bréfuel, Prof. Dr. S. Shova, F. Dahan, M. Verelst, Prof. Dr. J.-P. Tuchagues
Laboratoire de Chimie de Coordination du CNRS, UPR 8241
205 route de Narbonne, 31077 Toulouse Cédex (France)
Fax: (+33) 561-553-003
E-mail: tuchague@lcc-toulouse.fr

[b] Dr. J. A. Wolny, Dr. H. Paulsen, Prof. Dr. A. X. Trautwein
Institut für Physik, Universität zu Lübeck
Ratzeburger Allee 160, 23538 Lübeck (Germany)
Fax: (+49) 451-500-4214
E-mail: paulsen@physik.uni-luebeck.de
trautwein@physik.uni-luebeck.de

[c] G. Lemercier
Present address: École Normale Supérieure de Lyon
Laboratoire de Chimie UMR CNRS and ENS-Lyon no. 5532
46 allée d'Italie, 69364 Lyon Cédex 07 (France)

[d] M. Verelst
Present address: Centre d'Elaboration de Matériaux et d'Etudes Structurales, UPR CNRS 8011
29 rue Jeanne Marvig, 31055 Toulouse Cédex (France)

[e] Prof. Dr. S. Shova
On leave from the Institute of Applied Physics
Academy of Sciences of Moldova
Academiei Street 3, 2028 Chisinau (Moldova)

[f] Dr. J. A. Wolny
On leave from Wydzial Chemii, Uniwersytet Wroclawski
Joliot-Curie 14, 50-383 Wroclaw (Poland)

Introduction

The present knowledge of the molecular mechanism of the spin-crossover (SCO) phenomenon does not yet allow monitoring of such intrinsic characteristics of a SCO material as its transition temperature ($T_{1/2}$), cooperativeness and frequency of spin-state conversion. It is, however, clear that this would be highly desirable in view of the possible applications, and many studies have already been accomplished with this aim.[1] The cubic crystal field determines the energy minima for the low-spin (LS) and high-spin (HS) potential surfaces of d^4, d^5, d^6, and d^7 ions in octahedral ligand environments. An entropy-driven SCO may be observed when the energy gap between the LS and HS potential minima is comparable to kT. However, the crystal field does not depend exclusively on the direct ligand environment, but also on the further-distance environment. The latter possibly includes out-of-sphere ions and/or solvent molecules, which interact together and with the SCO molecules or complex cations in different possible ways: hydrogen bonds, ring stackings and van der Waals interactions, which constitute the "communication network" and determine the crystal packing.

To obtain SCO materials with chosen characteristics that allow their use for selected applications, the metal centers are required to be surrounded with chemical species that allow simultaneous monitoring of the intra- and intermolecular effects. The synthesis and use of a unique chemical species able to control both effects is an elegant and efficient approach.[2] However, in this approach it is extremely difficult to independently vary the intra- and intermolecular effects. As a more accessible approach we considered interconnecting two types of chemical species. The first type (neutral polydentate ligand) was selected to yield the appropriate ligand field range to the metal ion (intramolecular function). Suitable weak interactions were generated with a second type of chemical species (out-of-sphere anions), the functions of which are to allow fine-tuning of the ligand field and to participate in intermolecular interactions with the first type of species (communication network).

As the most favorable case for unambiguous experimental observation of the SCO phenomenon is the d^6 configuration, where the LS system is diamagnetic and the change in the number of unpaired electrons is four, we focused our attention on iron(II) systems. Experimental realization of the SCO phenomenon is determined by the availability of LS and HS states separated by only a few hundred reciprocal centimeters,[3] and therefore few ligand environments are able to produce the appropriate crystal field on the iron(II) center. Indeed, with very few exceptions,[4] ferrous SCO materials include an FeN_6 coordination sphere. However, there are several ways to obtain such a donor set, including the use of hexadentate ligands having an N_6 donor set or almost any combination of mono-, bi-, tri-, and tetradentate nitrogen ligands, including monoanions such as NCS^- or $NCSe^-$.[5]

Interestingly, the building block of several ferrous SCO materials characterized by an FeN_6 coordination sphere is an $[Fe^{II}(L_{bidentate})_3]^{2+}$ or $[Fe^{II}(L_{tridentate})_2]^{2+}$ complex cation that requires the presence of out-of-sphere anions to compensate its $2+$ charge. Several authors have shown that the characteristics of the $^1A_1 \rightleftarrows {}^5T_2$ SCO in the corresponding $[Fe^{II}(L_{bidentate})_3]X_2 \cdot (solvent)_n$[6–17] and $[Fe^{II}(L_{tridentate})_2]X_2 \cdot (solvent)_n$[18–24] materials depend on the nature of the out-of-sphere anions and the nature and number of solvent molecules. However, no correlation was found between any property of the considered anions and/or solvent molecules and any characteristic of the SCO. In most of the aforementioned studies, two to three factors effecting the communication between the ferrous building blocks vary simultaneously (nature of the out-of-sphere anions, nature and number of solvent molecules, nature and number of ligand atoms being able to participate in the communication between adjacent molecules). It is thus understandable that the resulting variation in the characteristics of the SCO was not rationalized for the studied materials.

Consequently, the following consideration has directed us in selecting a ligand suitable for carrying out this study: a dense 3D network of intermolecular interactions between the out-of-sphere anions and the complex cations is required to obtain an efficient communication network inside the SCO material. Bidentate or tridentate ligands that include nitrogen donors and bear a large number of outer NH functions are the best candidates for establishing such a network of hydrogen bonds. The simplest ligands fulfilling these criteria are the biimidazole ligands **I**–**IV** represented in Scheme 1. However, $bimH_2$ (**I**),[25] 4-bim (**II**),[26] and 2-bim

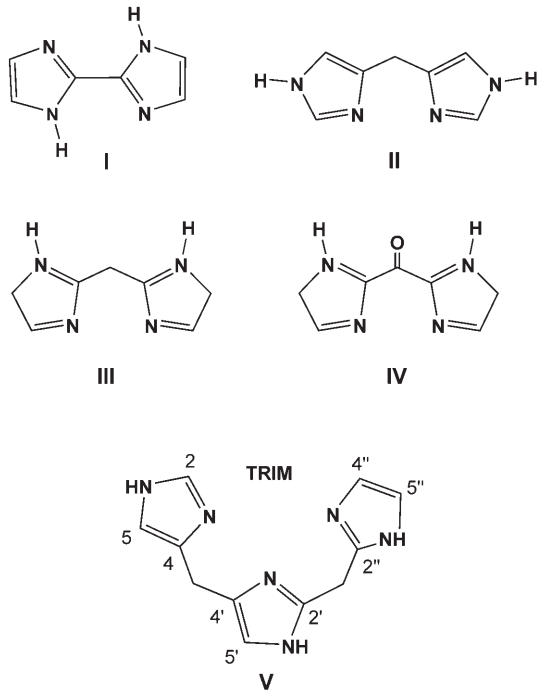

Scheme 1. Schematic drawings of some bi- and triimidazole ligands: $bimH_2$ (**I**), 4-bim (**II**), 2-bim (**III**), 2-bik (**IV**), and trim (**V**).

(**III**)[26] afford HS Fe^{II} complexes, whereas 2-bik (**IV**)[27] is the only ligand in this series that affords Fe^{II} SCO compounds. The X-ray crystal structure of $[Fe^{II}(Me_2\text{-}2\text{-}bik)_3](BF_4)_2$ shows that the ketonic oxygen atom is close to both N-CH_3 carbon atoms of Me_2-2-bik,[28] which suggests likely disturbances in the "out-of-sphere anion"–NH interactions induced by the ketonic oxygen atom for the parent ligand **IV**.

Among the tridentate ligands fulfilling the aforementioned criteria, the 4-(4-imidazolylmethyl)-2-(2-imidazolylmethyl)imidazole ligand[29] (trim, **V**, Scheme 1) has yielded interesting preliminary results[30] and was thus selected for carrying out this study. From this triimidazole ligand, several series of ferrous SCO complexes of general formula $[Fe^{II}(trim)_2]X_2$, $[Fe^{II}(trim)_2]XY$ or $[Fe^{II}(trim)_2]Z$ were prepared, characterized and studied. They included either identical X or different X and Y monoanions, or a unique Z dianion, as counterions. An extensive study of the fluoride derivative $[Fe^{II}(trim)_2]F_2$, here referred to as complex **1**, has been published elsewhere.[31]

Herein, we report the synthesis, characterization, and properties of $[Fe^{II}(trim)_2]Cl_2$ (**2**), $[Fe^{II}(trim)_2]Br_2\cdot MeOH$ (**3**), and $[Fe^{II}(trim)_2]I_2\cdot MeOH$ (**4**). X-ray crystal structure determinations of **2** (50, 293 K) and **4** (293 K) were performed with the aim of shedding some light on the origin of the impressive variation in the intrinsic characteristics of the SCO phenomenon for this series of complexes. Reports on the physical properties of **2**[32] and **3**[33] have been published elsewhere.

For a long time all attempts to explain the SCO phenomenon on a microscopic level were based on ligand-field theory.[34] With respect to ab initio or density functional theory (DFT) calculations, SCO complexes are intricate objects. Ab initio methods turned out to be inappropriate for a proper description of the SCO phenomenon: simple approaches like the Hartree–Fock method fail because they neglect Coulomb correlation, which leads to a strong bias towards higher spin multiplicities. The more sophisticated methods that include larger parts of the Coulomb correlation are too demanding with respect to computer resources. They have been applied only to the most simple transition metal complexes such as $[Fe(H_2O)_6]^{2+}$.[35] On the other hand, DFT methods are used for SCO compounds with increasing success and are currently the method of choice in this field (see reference [36] for a recent review). DFT calculations are now able to predict with reasonable accuracy the geometry, Mössbauer parameters, normal modes of molecular vibrations, entropy differences and other molecular properties. DFT calculations can even be used to predict changes of the transition temperature with qualitative accuracy.[37] However, all calculations published so far suffer from a severe limitation: they are restricted to free molecules. One may conclude that the SCO phenomenon can be partially described on a molecular level. For a complete and quantitative description, however, the inclusion of intermolecular effects is essential. This may be achieved through electronic structure calculations with periodic boundary conditions. Owing to the large size of the unit cells of SCO materials, which usually contain a few hundred atoms, such calculations are extremely demanding and, to our knowledge, have never been performed before. Herein, we report DFT calculations for unit cells with periodic boundary conditions of the complexes $[Fe^{II}(trim)_2]X_2$ (X = F, Cl, Br, I; **1**–**4**), as well as for the isolated $[Fe^{II}(trim)_2]X_2$ complex molecules. These calculations allow for the first time the separation of inter- and intramolecular factors that govern the SCO phenomenon. In this way, electronic structure calculations in the field of SCO research have reached a new quality.

Results and Discussion

Syntheses and compositional studies: The analytical results, IR spectra and thermogravimetric analysis (TGA) measurements allow the formulation of complexes **1**[31] and **2** without solvent of crystallization. Complexes **3** and **4** include methanol of crystallization with an Fe/MeOH ratio of 1:1. The lack of solvent of crystallization in **1** and **2**, and the solvent content in **4**, are confirmed by the molecular structures.

Crystal structure of complexes 2 (50, 293 K) and 4 (293 K): The complex cation $[Fe^{II}(trim)_2]^{2+}$ of **2** at 50 K is shown in Figure 1. Chelation of one iron(II) center by two tridentate

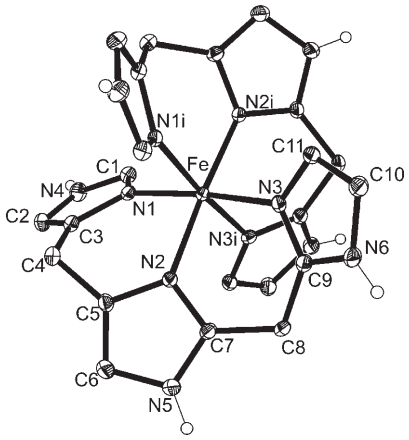

Figure 1. Molecular structure of the complex cation of $[Fe^{II}(trim)_2]Cl_2$ (**2**) at 50 K with atom labeling scheme. Thermal ellipsoids are drawn at the 50% probability level.

ligands (trim) yields the same type of complex cation $[Fe^{II}(trim)_2]^{2+}$ for complexes **2** (50, 293 K) and **4** (293 K), as previously observed for complex **1** at 293 K.[31] However, the Fe–N interatomic distances and angles collated in Table 1 indicate two different types of resulting FeN_6 coordination: 1) in complex **2** at 50 K and in **4** (293 K), all Fe–N distances are close to 2.0 Å and the N-Fe-N angles indicate almost perfect octahedral coordination; 2) in complex **1** (293 K) and in **2** at 293 K all Fe–N distances are close to 2.2 Å and the N-Fe-N angles indicate distorted octahedral coordina-

Table 1. Selected interatomic distances and angles for complexes **1**, **2**, and **4**.

out-of-sphere anion	F^-	Cl^-	Cl^-	I^-
temperature [K]	293	293	50	293
spin state	HS	HS	LS	<5% HS
Fe–N1 [Å]	2.180(3)	2.172(2)	1.9967(13)	1.996(5)
Fe–N2 [Å]	2.178(3)	2.170(2)	1.9942(13)	1.994(6)
Fe–N3 [Å]	2.186(3)	2.191(2)	1.9975(13)	1.994(5)
Fe–$N_{average}$ [Å]	*2.181*	*2.178*	*1.996*	*1.995*
N-Fe-N range [°]	81.6–102.2	82.6–100.3	86.6–95.1	87.5–93.5
ϕ[a] [°]	7.6	7.4	2.1	2.0
N···X [Å, av.]	2.626	3.137	3.142	3.690
Fe···Fe [Å]	8.43	8.67	8.52	8.44

[a] Average trigonal distortion as defined in reference [38].

tion. These results are in agreement with the Mössbauer and magnetic studies showing that, while complex **1** is HS at 293 K,[31] complex **2** exhibits an almost complete and smooth SCO between 80 and 260 K.[32] They also confirm that complex **4** is essentially LS at 293 K.[30] The coordinated nitrogen atoms define a rhombically distorted octahedron for the structures including HS iron(II), as indicated not only by the average trigonal distortion angles[38] $\phi = 7.6°$ (**1**) and 7.4° (**2**) at 293 K, but also by the absence of axial distortion (minute differences in Fe–N bond lengths).

The hydrogen-bond networks for the chloride (**2**) and iodide (**4**) complexes (Figure 2) are similar to that of the fluoride compound (**1**).[31] Each complex cation is connected to six halides through N–H···X bonds and conversely each halide is connected to three complex cations. The methanol molecule present in the iodide complex (**4**) is H-bonded to I^- (O1–H1···I), but is not involved in the hydrogen-bond network between $[Fe^{II}(trim)_2]^{2+}$ complex cations and I^- counter anions. The interatomic distances and angles characterizing these N–H···X hydrogen bonds are summarized in Table 1. The crystal packing primarily results from this dense system of hydrogen bonds, which organizes the $[Fe^{II}(trim)_2]^{2+}$ complex cations and X^- counter anions into nearly perpendicular interpenetrated sheets leading to the formation of a 3D network. In the case of the fluoride (**1**) and chloride (**2**) materials, the sum of the three H···X···H angles around each halide is close to 360° (359, 340, and 329° for **1**(HS), **2**(HS), and **2**(LS), respectively) and sizably higher than the sum of the three H···I···H angles (299°) observed for the iodide material. The departure of the halide from the plane of the sheet thus seems to be correlated to the size of the halide: while the smaller F^- ions fit almost perfectly the cavity between three $[Fe^{II}(trim)_2]^{2+}$ complex cations, larger X^- ions fit less well as their size increases, thus leading to an increase in intersheet distance with the size of the halide.

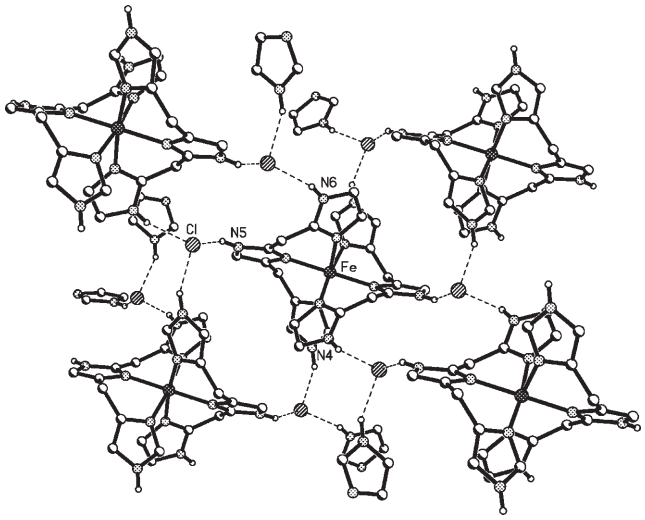

Figure 2. View of the 3D hydrogen-bond network of the complex $[Fe^{II}(trim)_2]Cl_2$ (**2**) at 50 K; the 3D hydrogen-bond network is similar for the fluoride compound (**1**) at 293 K, the chloride compound (**2**) at 293 K, and the iodide compound (**4**) at 293 K. For clarity, only one imidazole ring is shown for some neighboring complex molecules.

The N2-C5-C6-N5-C7 imidazole rings of molecules of the fluoride (**1**) and chloride (**2**) materials that reside in *ac* planes interact through π stacking with their centrosymmetrically related counterpart (staggered orientation). The interplanar distance between these overlapping imidazole rings is 3.58 (**1** (HS)), 3.52 (**2** (HS)), and 3.38 Å (**2** (LS)); these values associated with centroid-to-centroid distances of 3.71 (**1** (HS)), 3.86 (**2** (HS)), and 3.91 Å (**2** (LS)) indicate quite strong π-stacking interactions. For symmetry reasons, both N2-C5-C6-N5-C7 and N2i-C5i-C6i-N5i-C7i imidazole rings are involved in the same interaction: this leads to the formation of infinite chains of π-stacked $[Fe(trim)_2]^{2+}$ complex cations which develop along the [010] direction (Figure 3). As a result, the whole 3D communication network defined by the sheets of H-bonded molecules is additionally sustained by these π-stacking interactions. Although the N2-C5-C6-N5-C7 imidazole rings of centrosymmetrically related molecules of the iodide material (**4**) have the same staggered orientation, and in spite of their short interplanar distance of 3.12 Å, the value of their centroid-to-centroid distance (5.05 Å) indicates the absence of π-stacking interactions. At variance with **1** (F^-) and **2** (Cl^-), the 2D sheets of **4** are H-bonded to intercalated parallel layers formed by I^- counter anions and MeOH solvate molecules. In the structures of **1** and **2**, the counter anions are arranged practically within the 2D layers of $[Fe(trim)_2]^{2+}$ complex cations.

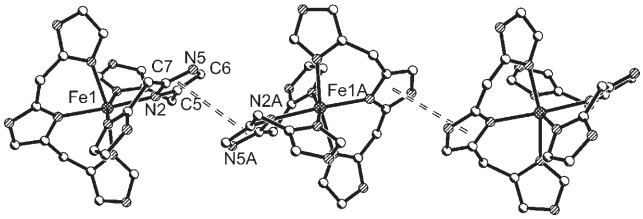

Figure 3. View of the 1D π-stacking network in the complex $[Fe^{II}(trim)_2]Cl_2$ (**2**) at 293 K; the 1D π-stacking network is similar for **2** at 50 K and for the fluoride compound (**1**) at 293 K.

The iron–iron distances between adjacent molecules (8.4–8.7 Å range, Table 1) are close to each other regardless of

the LS or HS state of the metal center and the size of the counter anions.

Magnetic properties: The thermal variation of the magnetic susceptibility measured for complex **4** in the 10–400 K temperature range is represented in Figure 4 as the $\chi_M T$ product

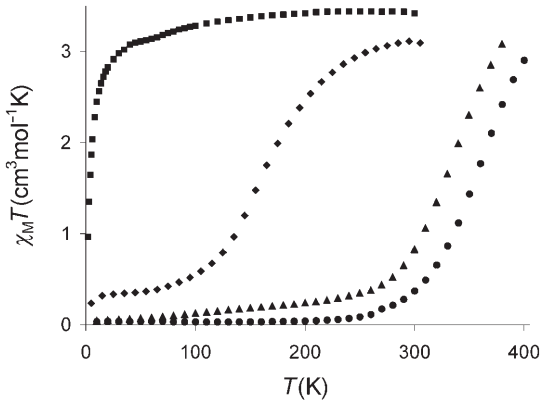

Figure 4. Thermal variation of the $\chi_M T$ product of $[Fe^{II}(trim)_2]F_2$, (**1**, ■), $[Fe^{II}(trim)_2]Cl_2$ (**2**, ◆), $[Fe^{II}(trim)_2]Br_2$·MeOH (**3**, ▲), and $[Fe^{II}(trim)_2]I_2$·MeOH (**4**, ●).

versus temperature. For comparison purposes, the thermal variation of the $\chi_M T$ product of **1**,[31] **2**[32] and **3**[33] is also represented in Figure 4. More or less gradual and complete SCO occurs for the four complexes in this series. The variety of magnetic behaviors is impressive considering that these compounds include the same complex cation and differ only for the out-of-sphere anions. The most striking observation is the large range of $T_{1/2}$ spanning from about 20 K for **1**[31] to about 380 K for **4**.

The thermal SCO of **1** occurs between about 120 and about 60 K; the sharp decrease of the $\chi_M T$ product below 30 K is due to zero-field splitting.[31] Complex **1** is a system with incomplete SCO occurring at low temperature, as a result of almost isoenergetic LS and HS levels, and which is monitored by molecular vibrations.[31] In this case, $T_{1/2} \approx 20$ K does not mean that SCO takes place at a temperature as low as about 20 K; instead it is a theoretical value meaning that if 50% of the iron sites could switch their spin, the temperature would then be about 20 K.

Mössbauer spectroscopy: The Mössbauer spectra of complexes **1**–**4** recorded in the 5–400 K temperature range consist of either one or two quadrupole doublets, depending on the compound and temperature.[30–33] They were least-squares fitted with Lorentzian lines, and the resulting isomer shift (δ), quadrupole splitting (ΔE_Q), and half-width of the absorptions ($\Gamma/2$) at selected temperatures are listed in Table 2. The δ and ΔE_Q values are in agreement with those previously published for the LS and HS states of iron(II) in other SCO compounds.

At intermediate temperatures, the contributions of the two spin states are well resolved and the spectra consist of two doublets in thermal equilibrium with each other. At low temperature, there are no observable line broadenings, which indicates that the HS⇄LS spin-state conversion rates in these compounds are slow compared to the hyperfine frequency ($\approx 10^8$ s^{-1}). Above 220 K for **2**, and 280 K for **3** and **4**, broadenings of the doublets indicate that the HS⇄LS conversion frequency reaches a value close to that of the hyperfine frequency.[39] Analysis of these line shapes with a two-state relaxation model based on the stochastic theory of line shapes[40] has been carried out for **2**[32] and **3**.[33] As a whole, the Mössbauer data are in agreement with the magnetic susceptibility results, thus confirming the presence of HS⇄LS crossover with a range of $T_{1/2}$ values larger than 300 K for this series of SCO complexes.

Qualitative analysis: A simple qualitative picture of the relationship between the nature of the out-of-sphere anion and the conversion temperature is suggested by the similarity of the hydrogen-bond networks in this series of complexes. The inductive effect of the anions is transmitted to the donor nitrogen atoms through the hydrogen bonds and imidazole rings (Scheme 2). Consequently, the basicity of the donor nitrogen atoms depends on the size of (charge density on) the out-of-sphere anions. In the case of the fluoride and chloride anions, for example, the stronger H···X hydrogen bond re-

Table 2. Observed Mössbauer parameters[a] for complexes **1**–**4**.

Compound	T [K]	LS component			HS component			
		δ	ΔE_Q	$\Gamma/2$	δ	ΔE_Q	$\Gamma/2$	γ_{HS}
$[Fe^{II}(trim)_2]F_2$ (**1**)	4.2	0.577(6)	0.16(1)	0.125(2)	1.148(4)	2.790(1)	0.123(1)	0.94
	77	0.571(8)	0.19(1)	0.125(2)	1.138(1)	2.827(2)	0.122(1)	0.95
	295	0.55[b]	0.23[b]	0.115(2)	1.022(1)	2.093(1)	0.123(2)	0.99
$[Fe^{II}(trim)_2]Cl_2$ (**2**)	80	0.551(2)	0.139(6)	0.130(4)	1.21(3)	2.67(7)	0.11(6)	0.04
	165	0.549(4)	0.12(2)	0.14(1)	1.109(6)	2.66(1)	0.16(1)	0.47
	293	0.497[b]	0.14[b]	0.7	1.018(2)	2.919(3)	0.131(3)	0.97
$[Fe^{II}(trim)_2]Br_2$·MeOH (**3**)	80	0.535(3)	0.134(1)	0.128(7)				0.00
	295	0.44(1)	0.18(6)	0.25(3)				≈0.00
	370	0.36(2)	0.15[b]		0.91(3)	1.4(3)		0.76
$[Fe^{II}(trim)_2]I_2$·MeOH (**4**)	80	0.532(5)	0.13(2)	0.14(1)				0
	293	0.466(4)	0.05(8)	0.20(2)				0

[a] The isomer shift (δ), quadrupole splitting (ΔE_Q), and half-width of the lines ($\Gamma/2$) are given in mm s^{-1}; statistical standard deviations are given in parentheses. [b] Fixed parameters.

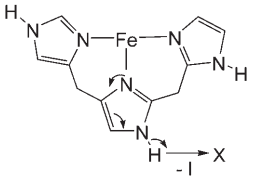

Scheme 2. Schematic representation of the $Fe_{1/2}$(trim)X asymmetric unit, which illustrates how the anion may exert an inductive effect on the metal center.

duces the electron density onto the lone pair of the donor nitrogen atom through the imidazole moiety. As a result, the iron–nitrogen bond is weakened; considering that the iron center is coordinated to six nitrogen donors experiencing the same effect, the HS state of Fe^{II} is stabilized.

Based on this qualitative analysis, an increased inductive effect of the out-of-sphere anion should correspond to a decreased SCO temperature $T_{1/2}$ for the halide-containing complexes. As shown in Figure 4, this is indeed the case. Furthermore, the $\chi_M T$ versus T curves for the chloride, bromide and iodide complexes illustrate another interesting point: their slope is very similar, which suggests that the cooperativity of their SCO (defined as $J/T_{1/2}$[41]) is very weakly or not correlated to this effect of the out-of-sphere anion.

The conversion temperature ($T_{1/2}$) depends on the ligand field, a local effect directly exerted onto the iron by the N_6 ligand environment. Considering that all complexes in this series include the same $[Fe(trim)_2]^{2+}$ complex cation, it is clear that the ligand field includes not only the constant contribution from the two trim ligands, but also a variable contribution originating from the only chemical species differing from one complex to the other. Consequently, the variation in $T_{1/2}$ results from the change in out-of-sphere anion transmitted by the unique set of atoms and bonds represented in Scheme 2, which may be considered as the "elementary communication wire" between the metal center and out-of-sphere anions.

Clearly the crystal packing, that is, the way in which elementary communication wires interconnect ferrous centers and out-of-sphere anions, together with the nature of the elementary communication wire, determines the cooperativity of the SCO. In the present series, the relative weakness of the elementary communication wires (which include an H···X hydrogen bond, and in the case of **1** and **2** a π-stacking interaction between imidazole rings) and the isotropic nature of the overall communication network (3D for **1** and **2**, 2D for **4** and, most probably, **3**) confer a significant elasticity to the crystal packing. These factors are most probably responsible for the weak cooperativity of the SCO in this series of materials.

To better understand these results and to check the possible role of the out-of-sphere anions in determining the spin state of Fe^{II} in $[Fe(trim)_2]^{2+}$ complex cations hydrogen-bonded to the different anions of the halide series, and possibly to shed some light on the nature of this counter-anion effect, the isolated $[Fe^{II}(trim)_2]X_2$ complex molecules **1**–**4** and the unit cell of the four materials were investigated at the DFT level.

DFT calculations: The calculations were performed within the local density approximation (LDA) for both the single molecules and the crystal lattices. The optimization for the LS and HS isomers of the neutral $[Fe(trim)_2]X_2$ molecules was carried out for all four anions. The starting geometries were those obtained for a given system in solid-state calculation, with the position of X^- taken such that one halide was H-bonded to the NH fragment of the central imidazole moiety of each ligand. The results obtained are collated in Table 3. The spin-state splitting E_S is the difference $E_{HS}-E_{LS}$ between the energy of the HS isomer and the energy of the LS isomer.

Table 3. Selected interatomic distances, angles, and spin-state splittings calculated for single molecules of $[Fe(trim)_2]X_2$.

Complex, spin state	Av. Fe–N [Å]	N-Fe-N range [°]	Av. N···H[a] [Å]	Av. N–X[a] [Å]	Av. H···X⁻ [Å]	E_s [kJ mol^{-1}]
$[Fe(trim)_2]F_2$, LS	1.87	87.2–92.1	1.511	2.50	1.03	50.9
$[Fe(trim)_2]F_2$, HS	2.05	85.6–96.5	1.426	2.42	1.04	
$[Fe(trim)_2]Cl_2$, LS	1.84	86.5–94.8	1.192	2.80	1.67	42.7
$[Fe(trim)_2]Cl_2$, HS	2.05	85.3–96.1	1.192	2.80	1.67	
$[Fe(trim)_2]Br_2$, LS	1.85	87.4–94.3	1.158	2.96	1.87	38.6
$[Fe(trim)_2]Br_2$, HS	2.05	85.4–96.2	1.156	2.96	1.87	
$[Fe(trim)_2]I_2$, LS	1.86	86.8–93.6	1.075	3.25	2.44	61.5
$[Fe(trim)_2]I_2$, HS	2.05	82.5–96.0	1.130	3.26	2.20	

[a] Central imidazole.

The values obtained for the free molecules do not reproduce the experimentally observed trend, but this could be reproduced by calculations for the crystals (by including periodic boundary conditions in the calculations; see below). A stronger stabilization of the LS state is obtained for complex **1** in particular, in comparison to the complexes **2** and **3**.

As shown in Figure 5, the bulk geometries of the complex cations deduced from the X-ray studies and those calculated are in fair agreement. The largest discrepancies concern the Fe–N bond distances: the calculated values of 1.84–1.86 and 2.05 Å for LS and HS molecules, respectively, are shorter than the experimental values lying in the ranges 1.99–2.015 and 2.17–2.19 Å, respectively. This finding may be understood as an effect of the intrinsic properties of the LDA approach, which is known to result in shortened metal–ligand bonds.[42] The pronounced stabilization of the LS isomer for **1** seems to be related to the distances of the hydrogen bonds: the F^-···H bonds are the shortest in the whole F^-, Cl^-, Br^-, I^- series, while the corresponding N···H distances

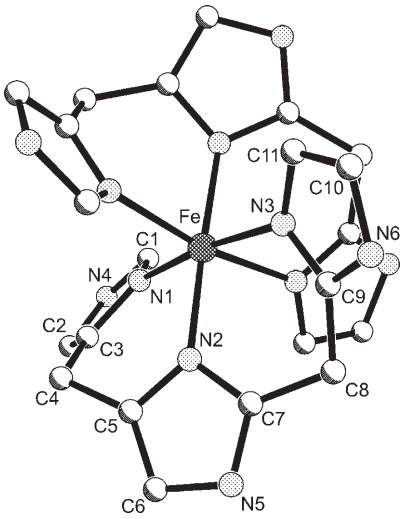

Figure 5. View of the complex cation in the calculated $[Fe(trim)_2]Cl_2$ HS structure of **2**.

reach the maximal values. This corresponds to an effective proton transfer to an anion: the H···F^- bond is shorter than the N–H bond. The above effect has a dramatic influence on the spin-state splitting, thus leading to an inversion of the experimentally observed stabilization of the LS state in the F^-, Cl^-, Br^-, I^- series. However, it is known that the calculations for N–H···X^- bonds in the gas phase reveal a tendency to shift the hydrogen atom towards the halide. This trend is counterbalanced by introducing the environment with a nonzero dielectric constant.[43] Moreover, in the solid, the X^- ions are involved in three or four hydrogen bonds and polarizability effects may play an important role. It is therefore clear that the observed dependence of the SCO properties on the anion may be explained only by considering the solid-state effects.

Calculations with periodic boundary conditions were also performed for the series of $[Fe^{II}(trim)_2]X_2$ complexes. For each system the calculations were carried out for a unit cell with either HS or LS complexes. All geometric parameters including the cell constants were optimized until the forces on all atoms became lower than a threshold value. The previously reported structure of the HS isomer of $[Fe^{II}(trim)_2]F_2$[31] and the structures of both isomers of $[Fe^{II}(trim)_2]Cl_2$ reported herein were used as a starting point for calculations of the respective complexes. Apart from that, calculations were performed for a pair of spin isomers of $[Fe^{II}(trim)_2]I_2$·MeOH with $Z=4$ (number of molecules per unit cell) starting from the structure reported here. The latter was also used as a starting point for the calculations for $[Fe^{II}(trim)_2]Br_2$·MeOH. To obtain the spin-state splitting E_S, the energy of a pure LS unit cell was subtracted from the energy of a pure HS unit cell and the resulting difference was divided by Z.

A comparison of calculated bond lengths and bond angles for complexes **1**–**4** with the available X-ray data (crystal structures, see above) shows again that the largest discrepancies concern the Fe–N bonds. The calculated Fe–N bond lengths lie in the range of 2.02 to 2.13 Å for HS **1**, 2.01 to 2.10 Å for HS **2**, 1.85 to 1.89 Å for LS **2** and 1.84 to 1.92 Å for LS **4**, whereas the experimental distances are in the ranges of 2.18–2.19, 2.17–2.19, 1.99–2.00, and 1.975–2.015 Å, respectively. The calculated N-Fe-N angles are closer to the observed ones: 83.0–100.6° for HS **1**, 86.0–93.7° for HS **2**, 85.6–95.4° for LS **2** and 87.7–93.7° for LS **4** (experimental values: 81.6–102.2, 82.7–100.3, 86.6–95.1 and 87.5–93.5°, respectively). Also, the value of the average trigonal twist angle ϕ for the calculated structures is in fair agreement with the experiment: the calculated values for HS **1**, HS **2**, LS **2**, and LS **4** are 3.7, 4.1, 2.4, and 2.1°, respectively (cf. Table 1). The CIF files for calculated structures are given in the Supporting Information.

Before discussing the packing effects it is important to note that we did not take into account the symmetry of the crystal in our calculations (i.e. the calculations are not bound to the space group of the starting geometry and are thus, in principle, able to predict the space group of the crystal).

The overall packing patterns observed by X-ray crystallography are well-reproduced by the calculations, as illustrated in Figures 6 and 7. The relevant interatomic distances are collated in Table 4. The crystal packings result primarily from the networks of hydrogen bonds, the orientations of

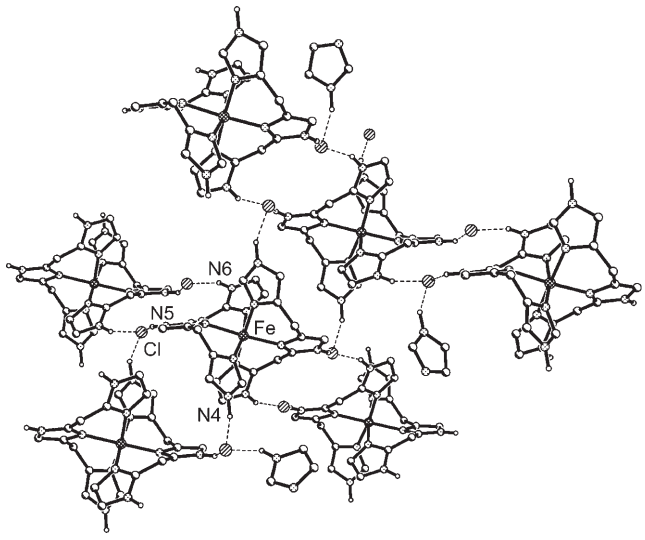

Figure 6. View of the 3D hydrogen-bond network for the calculated $[Fe^{II}(trim)_2]Cl_2$ HS structure of **2**.

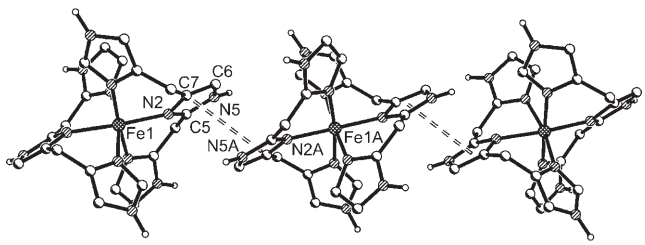

Figure 7. View of the 1D π-stacking network in the calculated $[Fe^{II}(trim)_2]Cl_2$ HS structure of **2**.

Table 4. Experimental and calculated intermolecular distances for the HS and LS lattices of $[Fe(trim)_2]X_2$ complex molecules [Å].

Complex, spin state	Calcd N···X	Exptl N···X	π-Stacking calcd	π-Stacking exptl
$[Fe(trim)_2]F_2$, LS	2.44–2.85		3.00[a] 3.34[b]	
$[Fe(trim)_2]F_2$, HS	2.49–2.71	2.61–2.66	3.02[a] 3.19[b]	3.58[a] 3.71[b]
$[Fe(trim)_2]Cl_2$, LS	2.95–3.01	3.13–3.15	3.10[a] 3.53[b]	3.38[a] 3.93[b]
$[Fe(trim)_2]Cl_2$, HS	2.94–2.99	3.13–3.15	3.07[a] 3.38[b]	3.52[a] 3.86[b]
$[Fe(trim)_2]Br_2$·MeOH, LS	3.19–3.55		2.38[a] 4.41[b]	
$[Fe(trim)_2]Br_2$·MeOH, HS	3.14–3.46		2.73[a] 4.22[b]	
$[Fe(trim)_2]I_2$·MeOH, LS	3.30–3.60	3.60–3.79	2.41[a] 4.71[b]	3.12[a] 5.05[b]
$[Fe(trim)_2]I_2$·MeOH, HS	3.34–3.63		3.28[a] 4.69[b]	

[a] Interplanar distance. [b] Centroid-to-centroid distance, in Å.

which are identical to those found in the X-ray structures of the corresponding complexes.

There seems to be some discrepancy between the observed and calculated sum of the three H···X···H angles around the halide, which is more pronounced for HS systems: the calculated values are 311, 301, 310, and 304° for **1** (HS), **2** (HS), **2** (LS), and **4** (LS), respectively. The increased number of accepted hydrogen atoms in the case of $X=I^-$ is also reproduced. Comparison of calculated and available experimental values for $N\cdots X^-$ distances corresponding to hydrogen bonds shows again that the calculated values are somewhat shorter than the observed ones. Both X-ray studies and calculations indicate that there is no change in hydrogen-bond lengths upon SCO.

The calculations display the presence of π-stacking interactions involving the N2-C5-C6-N5-C7 imidazole rings, observed for the fluoride (**1**) and chloride (**2**) materials. Both the interplanar distances and associated centroid-to-centroid distances are 0.3–0.6 Å shorter than those observed in X-ray structures (see Table 3). On the other hand, for the LS iodide material (**4**), in spite of the small interplanar distance (2.408 Å), the large centroid-to-centroid distance (4.71 Å) indicates the absence of π-stacking interactions, as established by X-ray methods. The same holds for $[Fe(trim)_2]Br_2$·MeOH (**3**). Thus, the calculations predict the determined 3D network for the fluoride (**1**), chloride (**2**) and iodide (**4**) materials, as well as the increased separation between 2D layers for **4**. In our opinion, the observed differences between the calculated and experimental interatomic distances are primarily due to Fe–N bond shortening within the LDA approach, as mentioned above.

The calculated energy differences (spin-state splitting E_s) between the HS and LS lattices of the four $[Fe(trim)_2]X_2$ complexes, together with the estimated values of transition temperatures $T_{1/2}$, are collated in Table 5. The trend observed for the calculated spin-state splitting E_S is in qualitative agreement with that observed for the transition temperatures. In other words, the calculations show that the strongest stabilization of the HS state is expected for the fluoride complex, which actually is essentially HS above $T=50$ K, while the most pronounced stabilization of the LS state is expected for $[Fe(trim)_2]I_2$·MeOH, in line with the experiment. Thus, for the first time, electronic structure calculations with periodic boundary conditions have been performed for SCO systems, which show the importance of intermolecular effects in tuning the ligand field and thus in determining the transition temperature.

Examination of the packing effects in the calculated structures allows the following description of the static and mechanical aspects of the lattices.

Table 5. Calculated spin-state splittings and cell volumes for HS and LS lattices of $[Fe(trim)_2]X_2$ complex molecules.

Anion	Spin state	V (exptl V) [Å^3]	$T_{1/2}^{calcd}$ ($T_{1/2}^{exptl}$) [K]	$[E_s]_X-[E_s]_F$ [kJ mol^{-1}]	E_s [kJ mol^{-1}]
F^-	HS	987 (1206)	– (<50)[31]	0	−47
	LS	954			
Cl^-	HS	1124 (1360)	90 (170–188)[32]	51.5	4.5
	LS	1057 (1270)			
Br^-[a]	HS	2368	390 (340)[33]	76.5	29.5
	LS	2294			
I^-[b]	HS	2471	510 (380)[c]	86	39
	LS	2353 (2921)			

[a] $[Fe(trim)_2]Br_2$·MeOH, $Z=4$. [b] $[Fe(trim)_2]I_2$·MeOH, $Z=4$. [c] Unpublished results.

For the calculated systems with $Z=2$, the packing corresponds to that observed by X-ray: the sheets formed by the H-bonded $[Fe(trim)_2]^+$ cations and X^- anions are connected into the 3D network, which is additionally sustained by the π-stacking interactions. In the F^-, Cl^-, Br^-, I^- series the increase in size of the anion results in a gradual increase of the intersheet distances, while the iron–iron distance within a sheet is unchanged. This finding is related to the pyramidal character of the $X^-\cdots(H)_3$ group of atoms in this series. Consequently, the centroid-to-centroid distance between the π-stacked imidazole rings increases in the series, thus leading to weakened interactions. The increased intersheet distance precludes π–π interactions and creates sufficient space to form methanol solvates in the case of the bromide and iodide systems.

The Fe–N bonds form an angle of about 45° with the plane of the sheets of H-bonded molecules, and thus the contraction of the coordination sphere upon HS-to-LS crossover induces an isotropic contraction of the complex cation resulting in an isotropic contraction of the whole 3D crystalline network through the N–H···X bonds. This contraction is associated with a "slippage" of the π-stacked imidazole rings of adjacent sheets.

Conclusion

The synthesis, characterization, and properties of $[Fe^{II}(trim)_2]Cl_2$ (**2**), $[Fe^{II}(trim)_2]Br_2$·MeOH (**3**), and [Fe^{II}-

$(trim)_2]I_2$·MeOH (**4**), including the X-ray crystal structure determinations of **2** (50, 293 K) and **4** (293 K), have been performed. In agreement with the magnetic susceptibility results, the Mössbauer data show the presence of HS⇄LS crossover with a range of $T_{1/2}$ larger than 300 K and spanning from ≈20 K for $[Fe(trim)_2]F_2$ (**1**) to ≈380 K for **4**. The conversion temperature ($T_{1/2}$) depends on the ligand field, a local effect directly exerted on the iron by the N_6 ligand environment. All the complexes in this series include the same $[Fe(trim)_2]^{2+}$ complex cation, and thus it is clear that the ligand field includes not only a constant contribution from the trim ligands, but also a variable one originating from the out-of-sphere anions and transmitted to the metal center by the connecting imidazole rings and hydrogen bonds.

As the hydrogen-bond network is similar for this series of complexes, which includes the same complex cation and differs only in the out-of-sphere anions, the impressive variation in the intrinsic characteristics of the SCO phenomenon is then interpreted as an inductive effect of the anions transmitted to the nitrogen donors through the hydrogen bonds and imidazole rings. The basicity of the nitrogen donor depends on the size of (charge density on) the out-of-sphere anion. Strong H···X hydrogen bonds reduce the electron density onto the lone pair of the nitrogen donor through the imidazole moiety. As a result, the iron–nitrogen bond is weakened. Considering that the iron center is coordinated to six nitrogen donors experiencing the same effect, the HS state of Fe^{II} is stabilized. Based on this rationale, an increased inductive effect of the out-of-sphere anion corresponds to a decreased SCO temperature $T_{1/2}$, in agreement with the experimental results.

The bulk geometries of the complex cations deduced from the X-ray studies and those calculated within the LDA approximation for both the single molecules and the crystal lattices at the DFT level are in fair agreement. However, while the trend for the spin-state splitting E_S (difference $E_{HS}-E_{LS}$ between the energy of the HS and LS isomers) calculated for the isolated molecules disagrees with the experimental one, the trend calculated with periodic boundary conditions agrees with that observed for $T_{1/2}$ of **1**–**4**. Indeed, the calculations predict the strongest stabilization of the HS state for the fluoride complex, which actually is essentially HS above $T=50$ K, while the most pronounced stabilization of the LS state is predicted for $[Fe(trim)_2]I_2$·MeOH, in line with the experiment. Thus, for the first time, electronic structure calculations with periodic boundary conditions have been performed for SCO systems, which show the importance of intermolecular effects in tuning the ligand field and thus in determining the transition temperature. Calculations using a GGA functional are currently being performed.

Experimental Section

Materials: All reagents and solvents were of analytical grade and were used without further purification. All syntheses involving Fe^{II} were carried out under a purified nitrogen atmosphere in an inert-atmosphere box (Vacuum Atmosphere HE 43-2) equipped with a dry train (Jahan EVAC 7). Solvents were degassed under vacuum prior to use.

Ligand: The 4-(4-imidazolylmethyl)-2-(2-imidazolylmethyl)imidazole ligand (trim) was synthesized as a faint-yellow microcrystalline powder.[29]

Fe^{II} complexes:

Caution! Perchlorate salts and complexes are potentially explosive and should be handled in small quantities and with much care.

*$[Fe^{II}(trim)_2]Cl_2$ (**2**)*: Compound **2** was obtained in the form of light-green crystals through direct reaction of ferrous chloride with the trim ligand. In a typical reaction, $FeCl_2·4H_2O$ (0.42 mmol) dissolved in the minimum amount of methanol was slowly added to trim (0.87 mmol) dissolved in the minimum amount of methanol under stirring. The reaction mixture was stirred for 48 h at room temperature and the minimum amount of acetonitrile necessary to induce crystallization was then added slowly. The resulting crystals were isolated by filtration 24 h later, washed with acetonitrile, dried under vacuum and stored in the inert-atmosphere box (yield: 110 mg, 70 %). Some of these crystals were of good enough quality for XRD measurements. Elemental analysis (%) calcd for $FeC_{22}H_{24}N_{12}Cl_2$ (583.3 g mol^{-1}): C 45.3, H 4.2, N 28.8, Cl 12.2, Fe 9.3; found: C 45.5, H 3.9, N 28.4, Cl 11.9, Fe 9.1. IR: $\tilde{\nu}=377$, 360, 344, 318 cm^{-1} (ν_{FeN}).

*$[Fe^{II}(trim)_2]Br_2$·MeOH (**3**) and $[Fe^{II}(trim)_2]I_2$·MeOH (**4**)*: Compounds **3** and **4** were obtained in the form of purple (**3**) and mauve (**4**) microcrystals through metathesis reactions similar to that described for **1**.[31] In a typical reaction, the chosen alkaline salt (2 mmol; LiBr for **3** and NaI for **4**) was slowly added as a solid under stirring to a freshly prepared, deep-purple methanolic solution (0.5 mmol) of $Fe^{II}(trim)_2(ClO_4)_2$.[31] The reaction mixture was stirred for 48 h at room temperature and a minimum amount of acetonitrile was subsequently added slowly to induce crystallization or precipitation. The resulting complex was isolated by filtration, washed with acetonitrile, dried under vacuum and stored in the glove box. Yield of **3**: 145 mg, 40 %. Elemental analysis (%) calcd for $FeC_{23}H_{28}N_{12}OBr_2$ (704.2 g mol^{-1}): C 39.2, H 4.0, N 23.9, Br 22.7, Fe 7.9; found: C 39.1, H 4.0, N 24.3, Br 22.4, Fe 7.8. IR: $\tilde{\nu}=3350$ (ν_{OH}), 1025 (ν_{CO}), 466, 440, 395, 329, 227 cm^{-1} (ν_{FeN}). Yield of **4**: 150 mg, 40 %. Elemental analysis (%) calcd for $FeC_{23}H_{28}N_{12}OI_2$ (798.2 g mol^{-1}): C 34.6, H 3.5, N 21.1, I 31.8, Fe 7; found: C 34.8, H 3.3, N 21.1, I 30.9, Fe 6.8. IR: $\tilde{\nu}=3350$ (ν_{OH}), 1025 (ν_{CO}), 435, 355, 328, 220 cm^{-1} (ν_{FeN}).

Physical measurements: Microanalyses for C, H, and N were performed by the Microanalytical Laboratory of the Laboratoire de Chimie de Coordination in Toulouse and for Cl, Br, I, and Fe, by the Service Central de Microanalyses du CNRS in Vernaison, France. Infrared spectra (4000–200 cm^{-1}) were recorded on a Perkin–Elmer 983 spectrophotometer coupled with a Perkin–Elmer infrared data station. Samples were run as CsBr pellets prepared under nitrogen in the dry box. TGA measurements were carried out with a Setaram TG-DTA92 apparatus coupled with a Leybold Heraeus QX 2000 mass spectrometer. Variable-temperature magnetic susceptibility data were obtained as previously described[44] on powdered microcrystalline samples with a Faraday-type magnetometer equipped with a continuous-flow Oxford Instruments cryostat or a Quantum Design MPMS superconducting quantum interference device (SQUID) magnetometer. Data were corrected for the contribution of the sample holder and diamagnetism of the sample.

Mössbauer measurements were obtained with a constant-acceleration conventional spectrometer using a 25-mCi source of ^{57}Co (Rh matrix). The absorber was a powdered sample enclosed in a 20-mm-diameter cylindrical, plastic sample holder, the size of which was determined to optimize the absorption. Variable-temperature spectra were obtained by using MD 306 (300–4.2 K) and DN1754 (300–400 K) Oxford cryostats, the thermal scanning being monitored by an Oxford ITC4 servocontrol device (±0.1 K accuracy). A least-squares computer program[45] was used to fit the Mössbauer parameters and determine their standard deviations of statistical origin (given in parentheses). Isomer shift values (δ) are relative to metallic iron at 293 K.

All samples used for physical or chemical characterizations were prepared inside a glove box under a purified nitrogen atmosphere. All necessary care was taken while transferring the samples to prevent any aerial oxidation. More particularly, the sample holders were sealed inside the glove box prior to their transfer to the SQUID or Mössbauer spectrometer.

Crystal structure determination of 2 and 4: X-ray data for compounds **2** and **4** were collected at 293 K on a CAD4 diffractometer (Enraf Nonius) using graphite-monochromated $Mo_{K\alpha}$ radiation ($\lambda = 0.71073$ Å). A light-green crystal of $[Fe^{II}(trim)_2]Cl_2$ (**2**; $0.50\times0.40\times0.30$ mm) was coated with Vaseline in an inert-atmosphere box and sealed in a Lindemann glass capillary. A mauve crystal of $[Fe^{II}(trim)_2]I_2\cdot MeOH$ (**4**; $0.55\times0.50\times0.25$ mm) was mounted in a similar way. The crystals were then transferred to the diffractometer. Lattice parameters of the two compounds were obtained from a least-squares analysis of 25 carefully centered reflections with $12.6° < \theta < 20.3°$. The data were collected at ambient temperature using the $\omega-2\theta$ scan technique at variable rates. 2524 unique reflections were collected up to 25° for **2**, space group *P*2/*n*, and 3176 unique reflections were collected for **4** up to 27°, space group *Pccn*. The quality of the crystals was monitored by scanning three standard reflections every 2 h. No significant variation was observed during data collection. The data were corrected for absorption, Lorentz and polarization effects using the MolEN package for **2** and **4**.[46] Absorption corrections from psi scans were applied (**2**: $T_{min} = 0.9455$, $T_{max} = 0.9999$; **4**: $T_{min} = 0.7914$, $T_{max} = 0.9989$).[47]

X-ray data for compound **2** were collected at 50(2) K with an Oxford Diffraction Xcalibur CCD diffractometer using graphite-monochromated $Mo_{K\alpha}$ radiation and a Helijet cooler device from Oxford Instruments. The crystal was placed 60 mm from the CCD detector. More than the hemisphere of reciprocal space was covered by combination of four sets of exposures; each set had a different angle ϕ (0, 90, 180, 270°). Coverage of the unique set was 99.8 % complete up to $2\theta = 64°$. The unit cell determination and data integration were carried out using the CrysAlis package from Oxford Diffraction.[48] Intensity data were corrected for Lorentz and polarization effects.

All structures were solved by direct methods using SHELXS-97[49] and refined by full-matrix least-squares methods on F_o^2 with SHELXL-97[50] with anisotropic displacement parameters for non-hydrogen atoms. All H atoms attached to carbon were introduced in idealized positions using the riding model with their isotropic displacement parameters fixed at 110 % of their riding atom. Scattering factors were taken from the standard compilation.[51] The molecular plots were obtained using the ZORTEP program.[52] Relevant crystallographic data and refinement details are summarized in Table 6.

CCDC-285836 (**2**, 293 K), CCDC-285837 (**2**, 50 K), and CCDC-285838 (**4**, 293 K) contain the supplementary crystallographic data for this paper. These data can be obtained free of charge from the Cambridge Crystallographic Data Centre via www.ccdc.cam.ac.uk/data_request/cif.

Computational details for DFT calculations: Density functional calculations were performed with the local density approximation (LDA) using the Perdew–Zunger parametrization,[53] as implemented in the SIESTA program.[54,55] For the valence electrons, a polarized double-zeta basis set was used that consists of finite-range pseudo-atomic orbitals (PAOs).[56] An energy cutoff of 70 Rydberg was used for the interstitial charge density. The core electrons were described by pseudopotentials of the Troulliер–Martins type.[57] Calculations with periodic boundary conditions were performed for complete unit cells of $[Fe(trim)_2]X_2$. In addition, calculations were performed for an isolated $[Fe(trim)_2]^{2+}$ complex cation. A threshold value of 10^{-4} was chosen for the self-consistent field convergence. The atomic positions in the unit cell and the cell parameters were optimized up to a force tolerance of 2000 kJ mol^{-1} Å. The transition temperatures were derived on the basis of calculated E_S values and the vibrational entropy differences, calculated on the basis of normal vibration frequency calculations for isolated HS and LS isomers of $[Fe(trim)_2]^{2+}$ complex cations performed with the Gaussian 03 program.[58]

Table 6. Crystallographic data and refinement parameters for compounds **2** and **4**.

	$[Fe^{II}(trim)_2]Cl_2$ (**2**)	$[Fe^{II}(trim)_2]Cl_2$ (**2**)	$[Fe^{II}(trim)_2]I_2\cdot MeOH$ (**4**)
formula	$C_{22}H_{24}N_{12}Cl_2Fe$	$C_{22}H_{24}N_{12}Cl_2Fe$	$C_{23}H_{28}N_{12}OI_2Fe$
formula weight	583. 28	583.3	798.22
crystal system	monoclinic	monoclinic	orthorhombic
space group	*P*2/*n* (No. 13)	*P*2/*n* (No. 13)	*Pccn* (No. 56)
a [Å]	10.3436(11)	10.2203(16)	8.729(3)
b [Å]	8.6719(10)	8.5154(12)	19.829(3)
c [Å])	15.1686(14)	14.6286(12)	16.878(3)
β [°]	92.068(13)	94.133(11)	90
V [Å^3]	1359.7(2)	1269.8(3)	2921.4(11)
Z	2	2	4
T [K]	293	50	293
$\rho_{(calcd)}$ [mg/m^3]	1.425	1.526	1.815
F(000)	600	600	1560
$\lambda(Mo_{k\alpha})$ [Å]	0.71073	0.71073	0.71073
crystal size [mm]	$0.50\times0.40\times0.30$	$0.45\times0.30\times0.20$	$0.55\times0.50\times0.25$
μ_{Mo} [mm^{-1}]	0.787	0.843	2.670
refl. measured	2524	11330	317
refl. unique/independent	2392	4198 [*R*(int) = 0.0436]	3176
refined parameters	168	168	184
GOOF on F^2	1.034	0.998	0.905
R [$I > 2\sigma(I)$][a]	0.0255	0.0403	0.0289
wR[b]	0.0722	0.1007	0.0928

[a] $R = \Sigma||F_o|-|F_c||/\Sigma|F_o|$. [b] $wR = [\Sigma w(|F_o^2|-|F_c^2|)^2/\Sigma w|F_o^2|^2]^{1/2}$.

Acknowledgements

Financial support by the Deutsche Forschungsgemeinschaft (DFG) (Tr 97/31 and Tr 97/32) and by the CNRS-DFG collaborative programme are gratefully acknowledged.

[1] a) C. Jay, F. Grolière, O. Kahn, J. Kröber, *Mol. Cryst. Liq. Cryst.* **1993**, *A234*, 255; b) P. Gütlich, *Nucl. Instrum. Methods Phys. Res.* **1993**, *B76*, 387; c) P. Gütlich, A. Hauser, H. Spiering, *Angew. Chem.* **1994**, *106*, 2109; *Angew. Chem. Int. Ed. Engl.* **1994**, *33*, 2024; d) O. Kahn, J. C. Martinez, *Science* **1998**, *279*, 44; e) A. Hauser, J. Jeftic, H. Romstedt, R. Hinek, H. Spiering, *Coord. Chem. Rev.* **1999**, *190–192*, 471; f) S. Hayami, Z.-Z. Gu, H. Yoshiki, A. Fujishima, O. Sato, *J. Am. Chem. Soc.* **2000**, *123*, 11644; g) Y. Sunatsuki, Y. Ikuta, N. Matsumoto, H. Ohta, M. Kojima, S. Iijima, S. Hayami, Y. Maeda, S. Kaizaki, F. Dahan, J.-P. Tuchagues, *Angew. Chem.* **2003**, *115*, 1652; *Angew. Chem. Int. Ed.* **2003**, *42*, 1614.

[2] a) W. Vreugdenhil, J. H. van Diemen, R. A. G. de Graaff, J. G. Haasnoot, J. Reedijk, A. M. van der Kraan, O. Kahn, J. Zarembowitch, *Polyhedron* **1990**, *9*, 2971; b) A. Ozarowski, Y. Shunzhong, B. R. McGarvey, A. Mislankar, J. E. Drake, *Inorg. Chem.* **1991**, *30*, 3167; c) J. Kröber, E. Codjovi, O. Kahn, F. Grolière, C. Jay, *J. Am. Chem. Soc.* **1993**, *115*, 9810; d) J. A. Real, E. Andres, M. C. Munoz, M. Julve, T. Granier, A. Bousseksou, F. Varret, *Science* **1995**, *268*, 265; e) J.-F. Letard, P. Guionneau, L. Rabardel, J. A. K. Howard, A. E. Goeta, D. Chas-

seau, O. Kahn, *Inorg. Chem.* **1998**, *37*, 4432; f) Y. Garcia, O. Kahn, L. Rabardel, B. Chansou, L. Salmon, J.-P. Tuchagues, *Inorg. Chem.* **1999**, *38*, 4663; g) P. J. van Konningsbruggen, Y. Garcia, O. Kahn, L. Fournes, H. Kooijman, A. L. Spek, J. G. Haasnoot, J. Moscovici, K. Provost, A. Michalowicz, F. Renz, P. Gütlich, *Inorg. Chem.* **2000**, *39*, 1891; h) N. Moliner, C. Muñoz, S. Letard, X. Solans, N. Menendez, A. Goujon, F. Varret, J. A. Real, *Inorg. Chem.* **2000**, *39*, 5390; i) D. L. Reger, C. A. Little, A. L. Rheingold, M. Lam, L. M. Liable-Sands, B. Rhagitan, T. Concolino, A. Mohan, G. J. Long, V. Briois, F. Grandjean, *Inorg. Chem.* **2001**, *40*, 1508; j) V. Niel, A. L. Thompson, M. C. Munoz, A. Galet, A. E. Goeta, J.-A. Real, *Angew. Chem.* **2003**, *115*, 3890; *Angew. Chem. Int. Ed.* **2003**, *42*, 3760; k) C. M. Grunert, J. Schweifer, P. Weinberger, W. Linert, K. Mereiter, G. Hilscher, G. Wiesinger, P. J. van Koningsbruggen, *Inorg. Chem.* **2004**, *43*, 155.

[3] a) M. A. Robinson, J. D. Curry, D. H. Busch, *Inorg. Chem.* **1963**, *2*, 1178; b) L. J. Wilson, D. Georges, M. A. Hoselton, *Inorg. Chem.* **1975**, *14*, 2968.

[4] a) W. S. J. Kelly, G. H. Ford, S. M. Nelson, *J. Chem. Soc. A* **1971**, 388; b) W. Levason, C. A. McAuliffe, M. M. Khan, S. M. Nelson, *J. Chem. Soc. Dalton Trans.* **1975**, 1778; c) V. Petrouleas, J.-P. Tuchagues, *Chem. Phys. Lett.* **1987**, *137*, 21; d) D. Boinnard, A. Bousseksou, A. Dworkin, J.-M. Savariault, F. Varret, J.-P. Tuchagues, *Inorg. Chem.* **1994**, *33*, 271; e) A. Bousseksou, L. Salmon, F. Varret, J.-P. Tuchagues, *Chem. Phys. Lett.* **1998**, *282*, 209; f) G. Psomas, N. Bréfuel, F. Dahan, J.-P. Tuchagues, *Inorg. Chem.* **2004**, *43*, 4590.

[5] a) P. Gütlich, *Struct. Bonding (Berlin)* **1981**, *44*, 83; b) E. König, *Struct. Bonding (Berlin)* **1991**, *76*, 51; c) *Magnetism: A Supramolecular Function* (Ed.: O. Kahn), NATO ASI Series C, *vol. 484*, Kluwer, Dordrecht, **1996**; d) Y. Ikuta, M. Ooidemizu, Y. Yamahata, M. Yamada, S. Osa, N. Matsumoto, S. Iijima, Y. Sunatsuki, M. Kojima, F. Dahan, J.-P. Tuchagues, *Inorg. Chem.* **2003**, *42*, 7001; e) M. Yamada, M. Ooidemizu, Y. Ikuta, S. Osa, N. Matsumoto, S. Iijima, M. Kojima, F. Dahan, J.-P. Tuchagues, *Inorg. Chem.* **2003**, *42*, 8406; f) H. Ohta, Y. Sunatsuki, M. Kojima, Y. Ikuta, Y. Goto, N. Matsumoto, S. Iijima, H. Akashi, S. Kaizaki, F. Dahan, J.-P. Tuchagues, *Inorg. Chem.* **2004**, *43*, 4154; g) H. A. Goodwin, *Spin Crossover in Transition Metal Compounds I* (Eds.: P. Gütlich, H. A. Goodwin), *Top. Curr. Chem.* **2004**, 233, 59; h) G. J. Long, F. Grandjean, D. L. Reger, *Spin Crossover in Transition Metal Compounds I* (Eds.: P. Gütlich, H. A. Goodwin), *Top. Curr. Chem.* **2004**, 233, 91; i) P. J. van Koningsbruggen, *Spin Crossover in Transition Metal Compounds I* (Eds.: P. Gütlich, H. A. Goodwin), *Top. Curr. Chem.* **2004**, 233, 123; j) H. Toftlund, J. J. McGarvey, *Spin Crossover in Transition Metal Compounds I* (Eds.: P. Gütlich, H. A. Goodwin), *Top. Curr. Chem.* **2004**, 233, 151.

[6] G. A. Renovitch, W. A. Baker, *J. Am. Chem. Soc.* **1967**, *89*, 6377.

[7] M. Sorai, J. Ensling, K. M. Hasselbach, P. Gütlich, *Chem. Phys.* **1977**, *20*, 197.

[8] a) A. M. Greenaway, E. Sinn, *J. Am. Chem. Soc.* **1978**, *100*, 8080; b) A. M. Greenaway, C. J. O'Connor, A. Schrock, E. Sinn, *Inorg. Chem.* **1979**, *18*, 2692.

[9] B. A. Katz, C. E. Strouse, *J. Am. Chem. Soc.* **1979**, *101*, 6214.

[10] M. Mikami, M. Konno, Y. Saito, *Chem. Phys. Lett.* **1979**, *63*, 566.

[11] H. A. Goodwin, R. N. Sylva, *Aust. J. Chem.* **1968**, *21*, 83.

[12] R. J. Dosser, W. J. Eilbeck, A. E. Underhill, P. R. Edwards, C. E. Johnson, *J. Chem. Soc. A* **1969**, 810.

[13] D. M. L. Goodgame, A. A. S. C. Machado, *Inorg. Chem.* **1969**, *8*, 2031.

[14] a) Y. Sasaki, T. Shigematsu, *Bull. Chem. Soc. Jpn.* **1973**, *46*, 3438; b) Y. Sasaki, T. Shigematsu, *Bull. Chem. Soc. Jpn.* **1974**, *47*, 109.

[15] D. M. L. Goodgame, *Bull. Soc. Chim. Fr.* **1972**, 3.

[16] a) J. R. Sams, J. C. Scott, T. B. Tsin, *Chem. Phys. Lett.* **1973**, *18*, 451; b) J. R. Sams, T. B. Tsin, *J. Chem. Soc. Dalton Trans.* **1976**, 488; c) J. R. Sams, T. B. Tsin, *Inorg. Chem.* **1976**, *15*, 1544.

[17] A. T. Baker, H. A. Goodwin, *Aust. J. Chem.* **1977**, *30*, 771.

[18] a) R. N. Sylva, H. A. Goodwin, *Aust. J. Chem.* **1967**, *20*, 479; b) R. N. Sylva, H. A. Goodwin, *Aust. J. Chem.* **1968**, *21*, 1081; c) E. König, G. Ritter, H. A. Goodwin, *Chem. Phys.* **1973**, *1*, 17.

[19] H. A. Goodwin, R. N. Sylva, *Aust. J. Chem.* **1968**, *21*, 2881.

[20] H. A. Goodwin, D. W. Mather, *Aust. J. Chem.* **1972**, *25*, 715.

[21] K. H. Sugiyarto, D. C. Craig, A. D. Rae, H. A. Goodwin, *Aust. J. Chem.* **1993**, *46*, 1269.

[22] B. J. Sugiyarto, D. C. Craig, A. D. Rae, H. A. Goodwin, *Aust. J. Chem.* **1994**, *47*, 869.

[23] K. H. Childs, D. C. Craig, K. A. Ross, M. L. Scudder, H. A. Goodwin, *Aust. J. Chem.* **1994**, *47*, 891.

[24] M. J. Boylan, S. M. Nelson, *J. Chem. Soc. A* **1971**, 976.

[25] a) D. Boinnard, P. Cassoux, V. Petrouleas, J.-M. Savariault, J.-P. Tuchagues, *Inorg. Chem.* **1990**, *29*, 4114; b) M. A. Martinez Lorente, F. Dahan, V. Petrouleas, A. Bousseksou, J.-P. Tuchagues, *Inorg. Chem.* **1995**, *34*, 5346.

[26] G. Guillot, E. Mulliez, P. Leduc, J.-C. Chottard, *Inorg. Chem.* **1990**, *29*, 577.

[27] A. Bousseksou, C. Place, J. Linares, F. Varret, *J. Magn. Magn. Mater.* **1992**, *104–107*, 225.

[28] C. Place, PhD thesis, University of Paris XI–Orsay, France, **1993**.

[29] E. Mulliez, *Tetrahedron Lett.* **1989**, *30*, 6169.

[30] a) G. Lemercier, PhD thesis, University of Toulouse III, France, **1994**; b) G. Lemercier, A. Bousseksou, S. Seigneuric, F. Varret, J.-P. Tuchagues, *Chem. Phys. Lett.* **1994**, *226*, 289; c) G. Lemercier, M. Verelst, A. Bousseksou, F. Varret, J.-P. Tuchagues in *Magnetism: A Supramolecular Function* (Ed.: O. Kahn), NATO ASI Series C, *vol. 484*, Kluwer, Dordrecht, **1996**, p. 335.

[31] A. Bousseksou, M. Verelst, H. Constant-Machado, G. Lemercier, J.-P. Tuchagues, F. Varret, *Inorg. Chem.* **1996**, *35*, 110.

[32] G. Lemercier, A. Bousseksou, M. Verelst, J.-P. Tuchagues, F. Varret, *J. Magn. Magn. Mater.* **1995**, *150*, 227.

[33] A. Thiel, A. Bousseksou, M. Verelst, F. Varret, J.-P. Tuchagues, *Chem. Phys. Lett.* **1999**, *302*, 549.

[34] A. Hauser, *Spin Crossover in Transition Metal Compounds I* (Eds.: P. Gütlich, H. A. Goodwin), *Top. Curr. Chem.* **2004**, 233, 49.

[35] A. Fouqueau, M. E. Casida, L. M. L. Daku, A. Hauser, F. Neese, *J. Chem. Phys.* **2005**, *122*, 044110.

[36] H. Paulsen, A. X. Trautwein, *Spin Crossover in Transition Metal Compounds III* (Eds.: P. Gütlich, H. A. Goodwin), *Top. Curr. Chem.* **2004**, 235, 197.

[37] a) H. Paulsen, L. Duelund, A. Zimmermann, F. Averseng, M. Gerdan, H. Winkler, H. Toftlund, A. X. Trautwein, *Monatsh. Chem.* **2003**, *134*, 295; b) H. Paulsen, A. X. Trautwein, *J. Phys. Chem. Solids* **2004**, *65*, 793.

[38] H.-R. Chang, J. K. McCusker, H. Toftlund, S. R. Wilson, A. X. Trauwein, H. Winkler, D. N. Hendrickson, *J. Am. Chem. Soc.* **1990**, *112*, 6814.

[39] a) P. Adler, A. Hauser, A. Vef, H. Spiering, P. Gütlich, *Hyperfine Interact.* **1989**, *47*, 343; b) P. Adler, H. Spiering, P. Gütlich, *J. Phys. Chem. Solids* **1989**, *50*, 587.

[40] a) M. Blume, *Phys. Rev.* **1968**, *174*, 351; b) P. Adler, H. Spiering, P. Gütlich, *Hyperfine Interact.* **1988**, *42*, 1035.

[41] A. Bousseksou, L. Tommasi, G. Lemercier, F. Varret, J.-P. Tuchagues, *Chem. Phys. Lett.* **1995**, *243*, 493.

[42] W. Koch, M. C. Holthausen, *A Chemist's Guide to Density Functional Theory*, Wiley-VCH, Weinheim, **2000**, chap. 8.1.2.

[43] A. Abkowicz-Bienko, M. Biczysko, Z. Latajka, *Comput. Chem.* **2000**, *24*, 303.

[44] D. Luneau, J.-M. Savariault, P. Cassoux, J.-P. Tuchagues, *J. Chem. Soc. Dalton Trans.* **1988**, 1225.

[45] F. Varret, *Proceedings of the International Conference on Mössbauer Effect Applications, Jaipur, India, 1981*, Indian National Science Academy, New Delhi, **1982**.

[46] C. K. Fair, *MolEN: Structure Solution Procedures*, Enraf-Nonius, Delft, **1990**.

[47] A. C. T. North, D. C. Phillips, F. S. Mathews, *Acta Crystallogr. A* **1968**, *A24*, 351.

[48] CrysAlis RED, Oxford Diffraction Ltd., Version 1.170.32, **2003**.

[49] G. M. Sheldrick, SHELXS-97: Program for Crystal Structure Solution, University of Göttingen, Germany, **1990**.

[50] G. M. Sheldrick, SHELXL-97: Program for the Refinement of Crystal Structures from Diffraction Data, University of Göttingen, Germany, **1997**.
[51] *International Tables for Crystallography*, *vol. C*, Kluwer, Dordrecht, **1992**, Tables 4.2.6.8 and 6.1.1.4.
[52] L. Zsolnai, H. Pritzkow, G. Huttner, ZORTEP: Ortep for PC, Program for Molecular Graphics, University of Heidelberg, Germany, **1996**.
[53] J. P. Perdew, A. Zunger, *Phys. Rev. B* **1981**, *23*, 5075.
[54] D. Sánchez-Portal, P. Ordejón, E. Artacho, J. M. Soler, *Int. J. Quantum Chem.* **1997**, *65*, 453.
[55] J. M. Soler, E. Artacho, J. D. Gale, A. García, J. Junquera, P. Ordejón, D. Sánchez-Portal, *J. Phys. Condens. Matter* **2002**, *14*, 2745.
[56] E. Artacho, D. Sánchez-Portal, P. Ordejón, A. García, J. M. Soler, *Phys. Status Solidi B* **1999**, *215*, 809.
[57] N. Troullier, J. L. Martins, *Phys. Rev. B* **1991**, *43*, 1993.
[58] Gaussian 03 (Revision B.01), M. J. Frisch, G. W. Trucks, H. B. Schlegel, G. E. Scuseria, M. A. Robb, J. R. Cheeseman, J. A. Montgomery, Jr., T. Vreven, K. N. Kudin, J. C. Burant, J. M. Millam, S. S. Iyengar, J. Tomasi, V. Barone, B. Mennucci, M. Cossi, G. Scalmani, N. Rega, G. A. Petersson, H. Nakatsuji, M. Hada, M. Ehara, K. Toyota, R. Fukuda, J. Hasegawa, M. Ishida, T. Nakajima, Y. Honda, O. Kitao, H. Nakai, M. Klene, X. Li, J. E. Knox, H. P. Hratchian, J. B. Cross, C. Adamo, J. Jaramillo, R. Gomperts, R. E. Stratmann, O. Yazyev, A. J. Austin, R. Cammi, C. Pomelli, J. W. Ochterski, P. Y. Ayala, K. Morokuma, G. A. Voth, P. Salvador, J. J. Dannenberg, V. G. Zakrzewski, S. Dapprich, A. D. Daniels, M. C. Strain, O. Farkas, D. K. Malick, A. D. Rabuck, K. Raghavachari, J. B. Foresman, J. V. Ortiz, Q. Cui, A. G. Baboul, S. Clifford, J. Cioslowski, B. B. Stefanov, G. Liu, A. Liashenko, P. Piskorz, I. Komaromi, R. L. Martin, D. J. Fox, T. Keith, M. A. Al-Laham, C. Y. Peng, A. Nanayakkara, M. Challacombe, P. M. W. Gill, B. Johnson, W. Chen, M. W. Wong, C. Gonzalez, J. A. Pople, Gaussian, Inc., Pittsburgh, PA, **2003**.

Received: October 10, 2005
Revised: May 2, 2006
Published online: July 28, 2006

